POLITECNICO DI TORINO
Repository ISTITUZIONALE

Experimental investigation of the structural performance of fiber-reinforced patches in the repair of locally damaged steel pipes

*Original*
Experimental investigation of the structural performance of fiber-reinforced patches in the repair of locally damaged steel pipes / Da Silva, D.L., Echer, L., Rojo Tanzi, B.N., Marczak, R.J., Iturrioz, I.. - In: JOURNAL OF THE BRAZILIAN SOCIETY OF MECHANICAL SCIENCES AND ENGINEERING. - ISSN 1678-5878. - ELETTRONICO. - 45:8(2023), pp. 1-14. [10.1007/s40430-023-04348-x]

*Availability:*
This version is available at: 11583/3002170 since: 2025-08-05T16:12:32Z

*Publisher:*
Springer

*Published*
DOI:10.1007/s40430-023-04348-x

*Terms of use:*

This article is made available under terms and conditions as specified in the corresponding bibliographic description in the repository

*Publisher copyright*

(Article begins on next page)

19 November 2026

## Preprint Notification

This is a preprint version of the final work published as:

da Silva, D. L., Echer, L., Rojo Tanzi, B. N., Marczak, R. J., & Iturrioz, I. (2023). **Experimental investigation of the structural performance of fiber-reinforced patches in the repair of locally damaged steel pipes.**

Published in: *Journal of the Brazilian Society of Mechanical Sciences and Engineering*, Vol. 45(08), No. 435, pp. 1–14.
DOI: https://doi.org/10.1007/s40430-023-04348-x


## How to Cite the Published Work

**APA:**

da Silva, D. L., Echer, L., Rojo Tanzi, B. N., Marczak, R. J., & Iturrioz, I. (2023). Experimental investigation of the structural performance of fiber-reinforced patches in the repair of locally damaged steel pipes. *Journal of the Brazilian Society of Mechanical Sciences and Engineering*, 45(8), 435.

**MLA:**

da Silva, Daniel L., et al. "Experimental investigation of the structural performance of fiber-reinforced patches in the repair of locally damaged steel pipes." *Journal of the Brazilian Society of Mechanical Sciences and Engineering* 45.8 (2023): 435.

**BibTeX:**

```
@article{daSilva2023experimental,
  title     = {Experimental investigation of the structural
               performance of fiber-reinforced patches in the
               repair of locally damaged steel pipes},
  author    = {da Silva, Daniel L and Echer, Leonel and
               Rojo Tanzi, Boris N and Marczak, Rog{\'e}rio J
               and Iturrioz, Ignacio},
  journal   = {Journal of the Brazilian Society of Mechanical
               Sciences and Engineering},
  volume    = {45},
  number    = {8},
  pages     = {435},
  year      = {2023},
  publisher = {Springer},
  doi       = {10.1007/s40430-023-04348-x},
  url       = {https://link.springer.com/article/10.1007/s40430-023-04348-x},
}
```

# Experimental Investigation of the Structural Performance of Fiber-Reinforced Patches in the Repair of Locally Damaged Steel Pipes

Daniel L. da Silva[1], Leonel Echer[2,3*†], Boris N. Rojo Tanzi[2†], Rogério J. Marczak[2†] and Ignacio Iturrioz[2†]

[1]UPGN Rota 3 – GasLub, PETROBRAS - Petróleo Brasileiro S.A., Rodovia Estadual RJ-116 - Km 5,2, Itaborraí, 24841-203, Rio de Janeiro, Brazil.

[2]Department of Mechanical Engineering, Federal University of Rio Grande do Sul, Rua Sarmento Leite, 425, Porto Alegre, 90046-902, Rio Grande do Sul, Brazil.

[3]ISI Polímeros, Instituto SENAI de Inovação em Engenharia de Polímeros, Av. Pres. João Goulart, 682, São Leopoldo, 93030-090, Rio Grande do Sul, Brazil.

*Corresponding author(s). E-mail(s): leonel.echer@ufrgs.br; leonel.echer@senairs.org.br;
Contributing authors: daniel.luis@petrobras.com.br; boris.rojotanzi@ufrgs.br; rato@mecanica.ufrgs.br; ignacio.iturrioz@ufrgs.br;
†These authors contributed equally to this work.

**Abstract**

In the present work, we investigate the performance of fiber-reinforced patches in the repair of a locally damaged steel pipe. The specimen of the study was submitted to hydrostatic tests before damage and after repair. Damage was generated as a through-thickness cut acting diagonally to the pipe axis. The repair patch comprised twelve layers of fiberglass plain weave fabric aligned orthogonally to the pipe axis. The layers were divided into four distinct sizes and overlapped in a stepped configuration.The hydrostatic tests were conducted until the maximum admissible pressure for the undamaged steel pipe. Two

piezoelectric sensors and four strain gauges were used in the pipe's instrumentation. The signal obtained during the successive tests was processed in terms of acoustic emission. The repair patch successfully survived the test scenario, and acoustic emission detected no significant events. The repair patch robustness was assessed by incrementally degrading its surface and resubmitting the repaired pipe to the hydrostatic test.The repair patch only failed after degrading half of its surface (middle and top layers). A liquid penetrant test was used to demonstrate the patch's failure (surface moisture evidencing leaking), which occurred in the borders of the through-thickness cut. Furthermore, the presence of microcracks or damage propagation in the surroundings of the substrate damage was not detected using a borescope.

**Keywords:** fiber-reinforced patch, structural repair, acoustic emission, hydrostatic test.

# 1 Introduction

Fiber-Reinforced Repair Patches (FRRP) are an excellent tool to extend the operational lifespan of locally damaged primary components [1]. Such a tool has been popular in the military sector since the '70s [2], and during the last decades, its use has expanded to commercial aircraft [3]. However, despite the rapid increase in the demand for such a tool, composite patches are still limited in conservative fields such as Oil & Gas, where the lack of comprehensive standards and regulations prevents more extensive use of adhesively bonded structural repairs. This industrial sector is particularly prone to costly maintenance breakdowns to correct faulty pipelines [4]. During such events, conventional repair procedures, e.g., welding, involve extended downtime and outages, which could be avoided using adhesively bonded repair patches.

## 1.1 Fiber-reinforced repair patches

Adhesively bonding composite textiles to the surface of locally damaged components efficiently increase the strength of such components [5, 6]. However, despite the broad use of such a tool in the last decades, there is no consensus on the best practices for achieving an "optimum" repair patch [7]. Parameters such as patch thickness, number of layers, fiber's orientation, and patch's geometrical shape and size are still subject of debate [1, 8]. The only point of agreement between different authors is that smaller patches are the best patches, i.e., minimal surface interference results in minor alterations of the original structure's inertia/stiffness and, consequently, minimal change in the structure's intrinsic mechanical response. This is particularly desirable in the aerospace and wind-energy sectors but stands true to any structural application of FRRP.

### 1.2 In situ repairing operations

If correctly applied, fiber-reinforced patches allow for a faster and easier way to perform field repairs of locally damaged metallic structures. Such a tool is an alternative to conventional welding operations, which inexorably result in costly maintenance breakdowns. However, despite the potential of adhesively bonded repair patches, their use in the Oil & Gas sector is still in its infancy compared to the aerospace sector. The development of technology comporting composite repair techniques for onshore applications began just after the 2000s [4]. Furthermore, these initial developments were carried out without assuring that the repair itself would not locally over-increase the pipe stiffness, making it prone to fracture due to stress concentrations at the end of the pipe-repair connection. However, it must be pointed out that in the past decade, considerable effort has been made to change this scenario and increase the use of composite repairs within the Oil & Gas industry.

Therefore, due to the lack of standardization for using small FRRP to restore degraded/damaged pipelines locally, the Oil & Gas sector represents a great field to test unorthodox approaches to increase the operational life of structures such as steel pipelines. Furthermore, this research topic may present colossal advancements in oil exploration during the next decades: decreasing downtimes, improving the operation's safety, and increasing productivity. All of these are key goals for the Oil & Gas industry (and any other part of the energy sector), especially when the world's attention is on energy self-sufficiency.

## 2 Methodology

All testings presented herein were conducted at the premises of the GasLub - *Polo de Gás e Lubrificantes*, a petrochemical complex owned and operated by PETROBRAS - *Petróleo Brasileiro S.A.* To assess the efficiency of repair patches with minimal surface extension, and, consequently, minimal stiffness/inertia modification of the substrate, a stepped repair patch was designed to repair a steel pipe.

The specimen consisted of a segment of hydrocarbon pipeline, following specifications from [9], with a nominal diameter equal to 101.6 mm (4"). The pipe counted a total length of 1.5 m and a wall thickness of 6.02 mm. The specimen was prepared for hydrostatic tests, as defined by [10] and [11]. Figure 1 shows a schematic drawing of the segment of a hydrocarbon pipeline custom-built for the present research. Table 1 exposes the pipeline specimen's components.

Further details regarding the specimen design and manufacturing process are presented in Appendix A. Figure 2(a) presents the finished specimen right after coating with a corrosion-resistant primer. Logically, this configuration is before the damage inclusion. Both Figures 2(b) and 2(c) detail the pipe instrumentation, which was added to the pipe *in-situ* during the preparation for the filed testings, which will be better discussed henceforward.

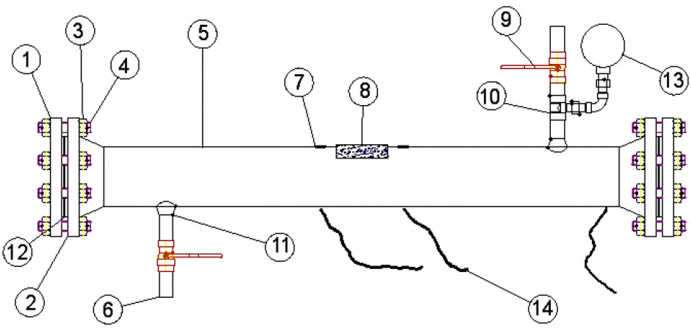



**Fig. 1** Test specimen's schematic drawing indicating each of its components.

**Table 1** Specimen design table.

| List of components | | |
|---|---|---|
| ID | Description | Qt. |
| 1 | blind flange 4" / #150 | 2 |
| 2 | weld Neck Flange 4" / #150 | 2 |
| 3 | M18 nut | 32 |
| 4 | M18 socket/case | 16 |
| 5 | pipe - API-5L Gr. B diam. 4" Sch 40 x 1m | 1 |
| 6 | pipe - 3/4" API-5L Gr. B diam. 3/4" | 2 |
| 7 | piezoelectric sensor | 2 |
| 8 | repair patch | 1 |
| 9 | spherical valve - 3/4" | 2 |
| 10 | T-joint diam. 3/4" x 1/2" | 2 |
| 11 | collar weld stud diam. 3/4" | 2 |
| 12 | spiral-wound gaskets | 2 |
| 13 | pressure gauge | 1 |
| 14 | sensors connection cables | 1 |

The damaged component is presented in detail in Figure 3(a), illustrating the through-thickness cut diagonally to the pipe axis. Figures 3(b) and 3(c) show the crack-like damage dimensions, which are given by the schematic of Figure 3(d): 49 mm × 5 mm on the outer surface and 21 mm × 5 mm on the inner surface. It is important to note that this difference in terms of damage length for the inner and outer pipe's surface is due to the circular geometry of the abrasive disk used to mechanically create the through-thickness cut, i.e., damage. The diagonal alignment of the crack-like damage was designed as being at 45° with the pipe's axial direction. The pipe surface was cleaned with acetone and then sanded (#80, #120, #200, and #400 grit sequentially) to remove irregularities produced during the cutting operation. The process to include damage and its subsequent surface preparation might result in a "blunt crack" scenario, hindering crack propagation. However, this is a price that must be paid since the damaged region preparation was intended to be trustworthy to the actual procedures that preceded the repair operation of

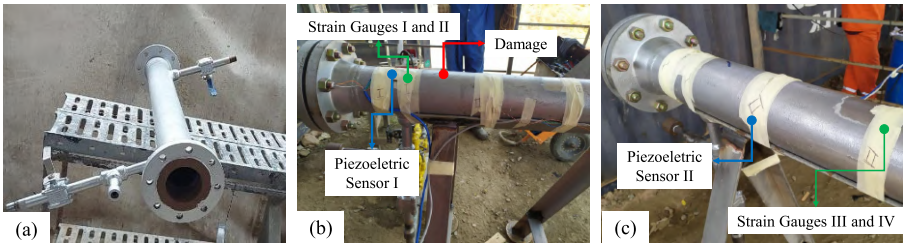



**Fig. 2** Specimen prepared to field tests: (a) pipeline segment prior to damage; (b) instrumentation attached to the pipe; and (c) sensors positioning and identification.

pipelines. Notwithstanding, this should not prevent microcracks initiation at the inner borders of the cut-like damage (end line left by the abrasion disk). Therefore, hydrostatic testing is assumed to achieve a sufficient stress level to promote such microcracks, whose occurrence is detectable through acoustic emission. Figure 3(e) presents the damaged region previously to the patching operation.

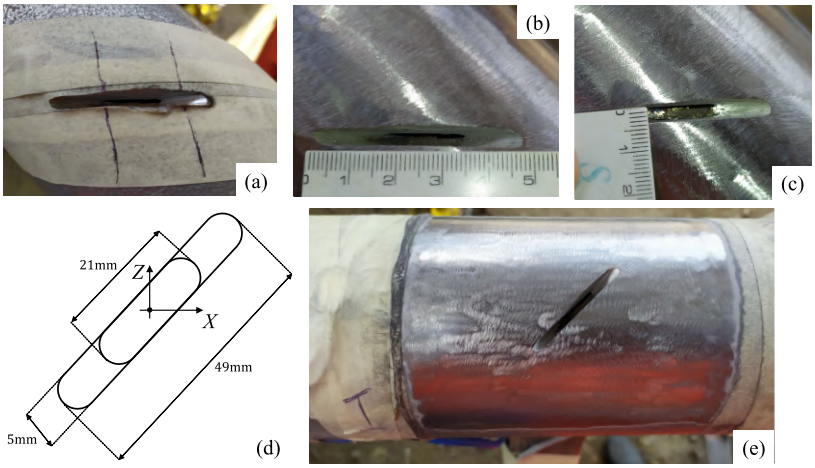



**Fig. 3** Crack-like, through-thickness cut, damage: (a) overall view; (b) length in detail; (c) crack opening in detail; (d) crack schematic; and (e) region prepared to receive the repair patch.

Within the Oil & Gas industry, a repair operation involving a scenario of through-thickness damage, as the one illustrated by Figure 3, is highly severe and very unlikely. Furthermore, according to the in-house N-2555 PETROBRAS standard [12], pipes subjected to thickness reductions must be strictly monitored with a periodic inspection plan based on the historical corrosion rate to determine if a safe operation can be guaranteed. In the case of 4" pipes made of carbon steel (as the one used herein), if a wall thickness inferior to 3.1 mm is detected, the safe operation must be ensured by a fracture mechanics study; otherwise, the operation of such a pipeline is not allowed

[12, 13]. Moreover, the API 570 standard [13] establishes that "longitudinal cracks should not be repaired through temporary repairs of any kind, whether welded or not welded, unless the piping engineer can demonstrate that there is no risk of crack propagation" of the defect under repair. Therefore, a repair operation involving a scenario of through-thickness damage, as illustrated by Figure 3, would be used only in very specific cases. However, we wanted to test the mechanical response of an FRRP in extreme situations, where a repair operation would even be prohibitive, and the in-house normative would recommend the complete replacement of the damaged component. Moreover, the reason for adopting diagonally aligned damage was to force a bidirectional stress scenario (combined stress state) acting on the extremities of the crack-like damage. The classic literature on fracture mechanics [14, 15] suggests a combined stress state at crack tips to test the direction changes that occur during the fracture propagation phenomena, i.e., maximum stress direction and minimum fracture toughness direction [16]. Such direction changes should differ considerably for a 45° crack regarding the direction of crack initiation and propagation.

The fiber-reinforced patch was defined as twelve layers of fiberglass plain weave fabric stacked in a stepped configuration. Each layer consisted of a perfectly square fabric ($l_p \times l_p$). The patch fabric's main directions (0/90) were aligned coincidentally with the pipe's axial ($X$) and tangential ($Z$) directions. The patch was designed as four overlapping slabs containing a specific number of layers per slab. The first slab (smaller in terms of area) comprised layers one to four, the subsequent slab encompassed layers five to seven, the third slab was formed by layers eight to ten, and the last slab was the largest, with layers eleven and twelve. The repair patch lay-up was defined as presented in Table 2. Such a stacking scheme was adopted to maximize the efficiency of the patch, ensuring a higher FRRP thickness in the region directly covering the crack-like surroundings and a lesser thickness far from the damaged central region, i.e., the patch's center. The design of the FRRP total thickness was based on the minimum thickness requirements suggested by international standards [17, 18].

**Table 2** Repair patch lay-up.

| Patch slab | Number of layers/slab | Layer size (total area) |
|---|---|---|
| | | $(l_p \times l_p)$ |
| $1^{st}$ (base) | 4 layers (0/90) | 3600 mm$^2$ |
| $2^{nd}$ (mid) | 3 layers (0/90) | 6400 mm$^2$ |
| $3^{rd}$ (mid) | 3 layers (0/90) | 10 000 mm$^2$ |
| $4^{th}$ (top) | 2 layers (0/90) | 14 000 mm$^2$ |

The patch's geometrical configuration adopted herein, as presented in Table 2, was selected to ensure a patch with minimal surface extension, an approach that goes in the opposite direction of the most common practices [17, 18]. A square FRRP was used to exploit the simplicity of using such

a patch geometry. The stepped stacking sequence was selected to avoid an abrupt transition from the inner layers (smaller) to the outer ones (larger). The transition rule adopted herein, $\approx 10\%$ variation in patch length between consecutive slabs, was considered practical and sufficiently small. Such a transition scheme is similar to the ones empirically achieved in the pioneer works developed in the '70s and '80s at the Australian Research Laboratories (ARL) [2, 19, 20]. If desired, a smoother configuration (scarf-like patch) could be achieved by reducing the number of layers per slab and increasing the total amount of slabs. The overall dimensions of the outer layer were defined to be at least twice the length of the crack-like damage, and the dimensions of the inner layers were defined to be only 10% to 20% larger than the square region encompassing the damage. Such a geometrical configuration was defined based on past testings [21] obtained for optimized patches on the repair of plates with partial or through-thickness damage.

Figure 4 presents the specimen after the repair operation. The patch was constituted of a plain weave fiberglass fabric ($200\,\mathrm{g\,m^{-2}}$) and an epoxy resin with micro-steel particulate reinforcement (4:1 mixture ratio). This type of resin [22] was selected due to its fast curing characteristics, i.e., the whole curing process took twelve hours at room temperature ($\approx 23\,^{\circ}\mathrm{C}$). To ensure a pressure distribution acting over the patch surface during the cure, the pipe's repaired region was enclosed by a thick layer (1.5 mm) of PVA plastic sheet involving the whole circumference. Over this PVA layer, a sequence of adjustable plastic clamps imposed pressure. It is important to note that since the patching operation was entirely performed in situ and due to the limited access to vacuum solutions, we could not enforce vacuum during the patch curing. The patching process was defined similarly to the one suggested by [23].

Four sensors were used to monitor the structure: two piezoelectric sensors at the surroundings of the damaged region, and two strain gauges applied directly on the pipe surface, one at the middle pipe and the other close to the damaged region. Figures 2(b) and 2(c) show the positioning of the aforementioned sensors.

Considering the pipe segment used as the test specimen, and according to the standards [10] and [9], the maximum allowable working pressure, $P_{max}$, for such specimen, was computed as 3 MPa (30 bar) and the maximum admissible testing pressure, $P_{TH}$, was defined [24, 25] as 7.84 MPa (79 bar). Therefore, four consecutive hydrostatic tests were performed. For each HT, the specimen was under different conditions:

- $1^{st}$ - Specimen undamaged: before damage and consecutive repairing operation, tested at $P_{TH}$;
- $2^{nd}$ - Specimen repaired with fiber-reinforced patch: patch as-applied without superficial degradation, tested at $P_{TH}$;
- $3^{rd}$ - Specimen with repair patch surface degraded by means of mechanical abrasion: 25 % of the layers removed (top one quarter), tested at $P_{TH}$;




**Fig. 4** Repaired region after the patch cure: (a) overview of the whole specimen; (b) close view of the patch external surface; and (c) patch after the first surface degrading procedure.

$4^{th}$ - Specimen with repair patch further degraded: 50 % of the layers removed (top half), tested until failure $P \leq P_{TH}$.

All tests were conducted alongside Acoustic Emission (AE) monitoring. The post-processing of the acquired signal was performed using tailored software [26] developed especially for the signal conditioning and post-processing needed in the present work. The AE employed a Butterworth filter (low-pass) in the range of 25 kHz and 100 kHz. Moreover, an attenuation of 60 dB for the intensity of the out-of-band signals and a steepness of 1 was used as an attempt to minimize the effect of noise over the analyzed signal.

# 3 Results and Discussions

The $1^{st}$ HT test aimed to identify any possible sealing inconsistencies on the specimen assembly at the testing bench. This first test was monitored, but only to assess the sensors and cables' integrity, since no acoustic emission event should take place. The $2^{nd}$ HT test was the first to effectively test the effectiveness of FRRP (in the $1^{st}$ the pipe was undamaged). After the $2^{nd}$ HT test, the repair patch surface was degraded subsequently to each testing regime. The specimen and, most importantly, the repair patch remained intact and without any deformation behavior suggesting internal crack/failure; this statement remained true even after the $3^{rd}$ test, at which only 75 % of the patch's layers (in terms of total thickness) were resisting load. The patch only failed during the $4^{th}$ HT, at a maximum testing pressure equal to $\approx 3.5$ MPa, which is $\approx 17$ % higher than the maximum allowed working pressure. It is very

important to stress that even after the patch was reduced to half its design thickness and 40 % of its original area (surface extension), it still resisted the maximum allowable working pressure. Moreover, the patch failed as a result of fluid permeation through the composite layers (visible droplets leaking at the patch surface), which was most likely caused by the presence of air bubbles trapped within the patch during the curing process.

Figure 5 illustrates the AE response obtained through the testing regimes. The graphics of such a figure combine the signal obtained using AE at two distinct conditions with the HT pressure curves. Figure 5(a) presents the signal at the maximum pressure of 7.84 MPa during the $1^{st}$ HT. Figure 5(b) shows the same result, but now for the $4^{th}$ HT. Note that the last HT testing sequence presents a lower pressure peak due to the patch failure during testing.

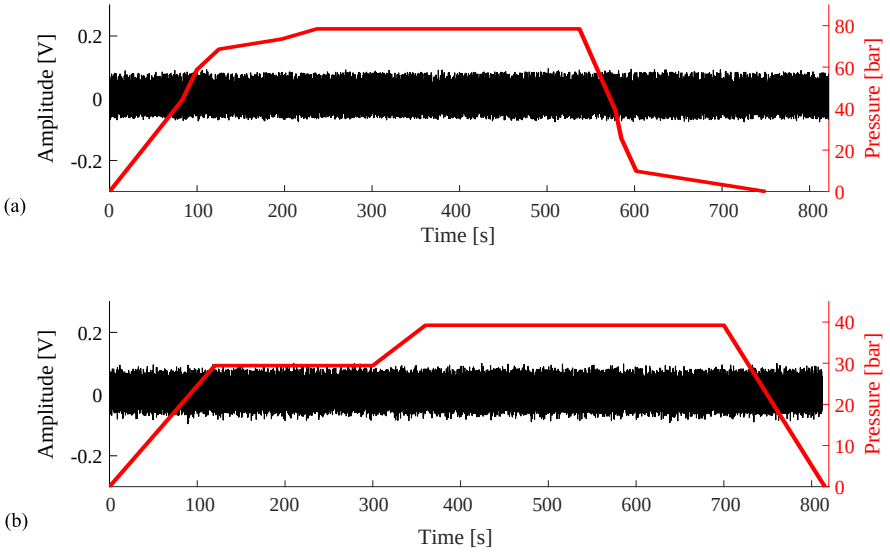



**Fig. 5** AE signal at peak testing pressures: (a) $1^{st}$ HT and (b) $4^{th}$ HT.

Even under extreme conditions, the signal response of the specimen (with a repair patch degraded up to 75 % of its original thickness) showed no significant events. This lack of events indicating internal crack/failure of the patch supports the efficiency of the technique adopted to repair the locally damaged pipe. Furthermore, the patch failure, during the $4^{th}$ HT, and the failure region were only visible after using penetrating fluid. Images of the FRRP surface after the penetrant fluid testing as exposed in Figure 6. The liquid penetrant tests showed that the two dot-like spots where the FRRP failure (leaking) took

place were exactly over the border between the through-thickness cut longitudinal edge and the central region of the patch. Such a position for the leaking is coherent with the patch bottom area that is subject to the maximum stress, i.e., the area directly covering the damage-like opening.

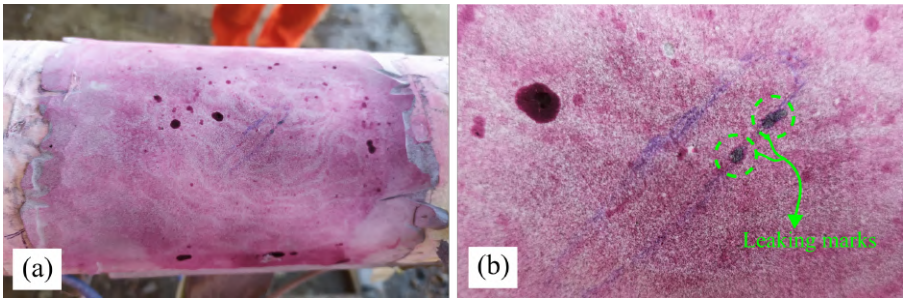



**Fig. 6** Penetrant fluid testings: (a) Overall patch surface; and (b) Detail view of the two point-like leak failure occurrences.

Appendix B presents pictures from the complementary non-destructive tests used. With the aid of a boroscope, the inner wall of the pipe was thoroughly checked in the vicinity of the damaged edges, searching for evidence of micro-cracks or some other indication of damage propagation. Different light spectrums were tested and, even after mechanically scrubbing the inner walls, no sign of visible defects (besides the through-thickness cut) was detected.

Since no characteristic AE event was identified in the data analyzed herein, an in-depth discussion regarding the failure mechanisms of the FRRP is not possible. Furthermore, the results obtained from the AE signal showed some influence of noise, despite the use of distinct tools to minimize such an effect. However, it is important to note that the tests were conducted in situ at the facilities of a petrochemical complex (still under construction at the time). Thus, the presence of heavy machinery and the huge amount of high-power welding machines connected to the same power grid that was supplied to the equipment used during the HT tests inherently resulted in the presence of noise in the AE signal. Appendix C presents a sequence of graphics generated through the AE signal processing.

# 4 Final Remarks

The present work experimentally investigated the use of FRRP for repairing damaged carbon steel pipelines submitted to internal pressure. The specimen preparation process was thoroughly documented in terms of designing, manufacturing, damaging, repairing, and testing. The whole damage procedure, i.e., through-thickness cut diagonally to the pipe axis, and the surface preparation prior to repair was conducted in such a manner to simulate real-life repairing operations within the Oil & Gas sector. The repair patching technique was

performed with a specific configuration (most geometrical parameters were empirically defined) to maximize the patch's mechanical efficiency. The FRRP consisted of fiberglass plain weave fabric and epoxy resin. Under hydrostatic pressure tests, the repair patch was effective, i.e., it supported the maximum admissible pressure without fail, and no significant event was detected by acoustic emission. Then, the repair surface was successively degraded through mechanical abrasion and retested until failure was detected, with superficial droplets indicating leaking on the patch's central region. The failure occurred only after the patch's extension was degraded to a state equal to half of its initial design condition.

Therefore, the results presented herein showed the efficiency of repairing locally damaged metallic structures. Such a statement proved true even under loading scenarios exceeding the design specifications of the tested specimen. The AE results corroborated the high efficiency of the fiber-reinforced patch, i.e., no dissipation events due to internal cracking was identified. The response obtained through the AE presented only the characteristic signal form of electrical noise, which indicates that an isolated power-supply system is a must for future tests.

Since only a failure by leaking was achieved herein, further tests are needed in order to comprehensively assess how a fragile-like fracture happens and what are the implications of severe loading scenarios to the overall performance of FRRP. Furthermore, given the precursor nature of the present research, only one specimen was tested, and there were no test repetitions for the consecutive HT tests presented herein. Thus, it was not possible to perform any statistical analysis.

The results of the tests conducted showed that the proposed approach is promising and could represent a step further in the direction of achieving a methodology to replace the conventional and costly welding repair operations for pipelines such as the one repaired in the present study.

## Declaration of Competing Interest

Besides the first author's employment relationship as an Equipment Engineer with the Brazilian company *PETROBRAS - Petróleo Brasileiro S.A.*, the authors declare no conflict of interest.

## CRediT author statement

DL da Silva: Conceptualization; Formal Analysis; Writing – original draft. L Echer: Conceptualization; Methodology; Supervision; Writing – review. BN Rojo Tanzi: Data curation; Software; Resources. RJ Marczak: Methodology; Formal Analysis. I Iturrioz: Conceptualization; Resources; Supervision.

## Acknowledgments

The authors are grateful to the engineering team working on the GasLub - *Polo de Gás e Lubrificantes* facilities at Itaboraí, RJ/BR, for supporting the present research and providing all the technical assistance to conduct the tests presented herein. The financial support offered by *Programa de Pós Graduação em Engenharia Mecânica* (PROMEC) and Brazilian funding agencies CAPES and CNPq is acknowledged as well.

## Appendix A Specimen Design

The present appendix provides additional information regarding the design of the specimen used for the in situ tests encompassed herein. Figure A1 shows distinct phases of the specimen's design. It is important to note that, in the construction of the pipeline segment all components/connections used were the very same employed in the hydrocarbon pipelines at the GasLub's facilities. Furthermore, all welding operations were conducted by highly skilled and certified welders. The whole process (design and testing) strictly followed the PETROBRAS in-house design codes and safety rules.

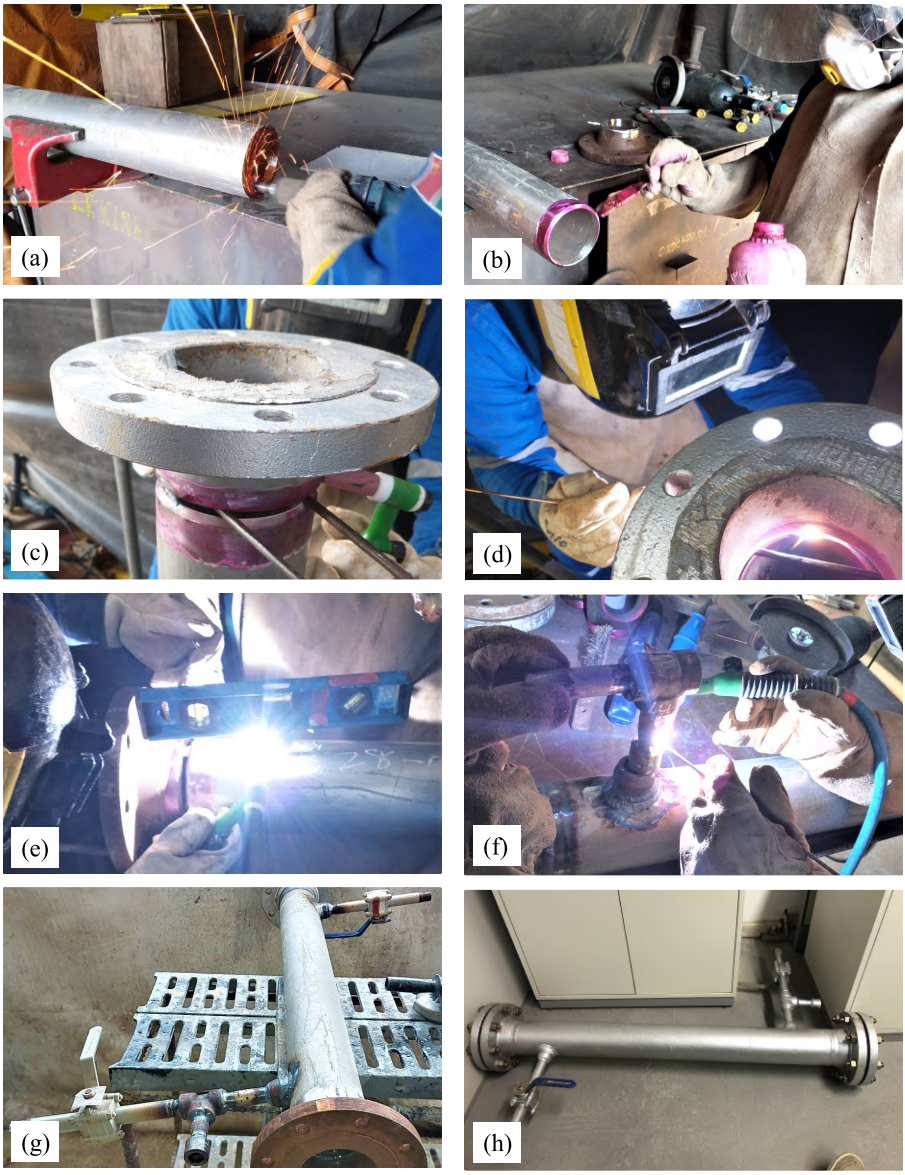



**Fig. A1** Specimen construction: (a) Pipe ends mechanical cleaning; (b) Surface preparation prior to welding; (c) Pipe ends assembly; (d) Pipe ends welding; (e) Alignment welding; (f) Valves assembly; (g) Pipe segment after welding; and (h) Specimen after primer protective coating.

# Appendix B Complementary Non-Destructive Tests

Figure B1 presents some pictures of the non-destructive tests conducted as complementary. The following images depict the pipe's inner wall inspection, which was achieved using a horoscope. Different light intensity and contrast levels were tested to obtain the best possible resolution for such pictures. None of the inner wall pictures showed any evidence of fracture evolution in the damage surroundings after the four HT sequences.

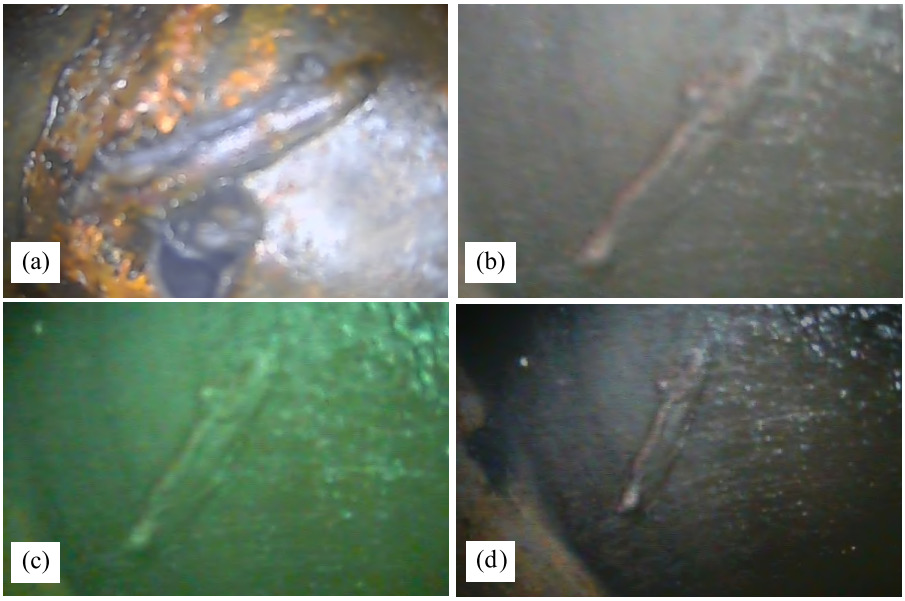



**Fig. B1** Complementary non-destructive tests- boroscope camera images: (a) Inner wall immediately after the last HT; (b) High contrast image; (c) Inner surface after scrubbing with low-intensity illumination; (d) Inner surface after scrubbing with normal illumination.

# Appendix C Acoustic Emission Signal Analysis

The following graphics are some of the acoustic emission signals obtained during the $3^{rd}$ HT, which should be the most relevant events. The graphics exposed below encompass pertinent portions (at specific time-frames $tf$) of the signal. The following graphics can be divided into two sets. The first one is the set of figures labeled with odd numbers (Figures C1 , C3, C5, C7, C9, C11, C13, C15, C17, C19, and C21). The second set comprehends the figures labeled with even numbers (Figures C2, C4, C6, C8, C10, C12, C14, C16, C18, C20, and C22). The set of oddly numbered figures presents the signal response (in blue) after going through the treatment and filtering procedures as presented in Section 2.

On the other hand, the set of evenly numbered figures is the signal response overlapped with a different filter (in red), in the range of 5 kHz to 25 kHz.

Only looking at the first set (odd numbers labeling), which comprehends a filter in the range of 25 kHz to 100 kHz, one could misinterpret the results as acoustic emission events. However, those are just noise and other signal perturbations induced in the system due to the ambient conditions discussed in Section 3. The second set (even numbers labeling) shows that the signal oscillations are coincident with what would be expected from the waveform of common electrical noise.

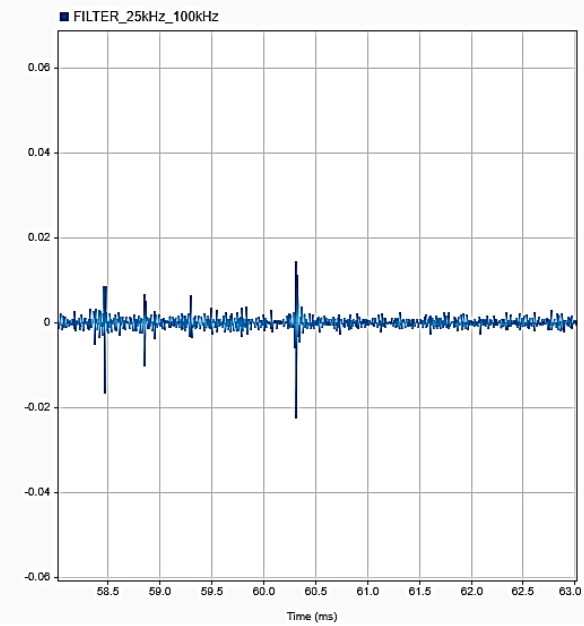



**Fig. C1** AE signal, $tf_1 = 58$ ms to 63 ms and filter range from 25 kHz to 100 kHz

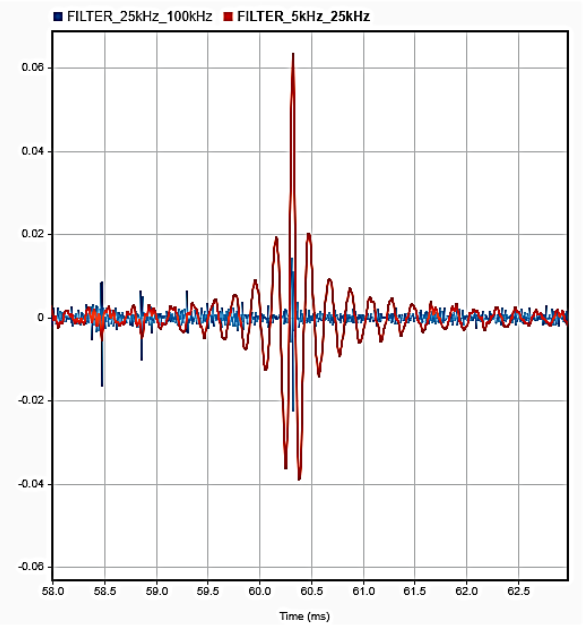



**Fig. C2** AE signal, $tf_1 = 58\,\text{ms}$ to $63\,\text{ms}$ and filter range from $5\,\text{kHz}$ to $25\,\text{kHz}$

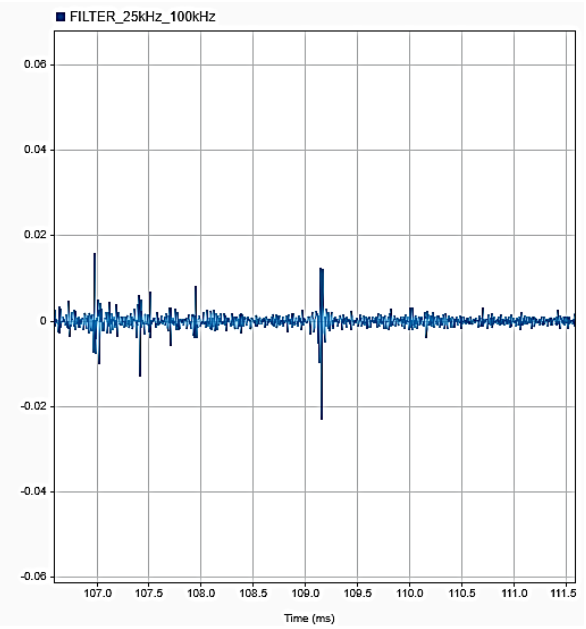



**Fig. C3** AE signal, $tf_2 = 107\,\text{ms}$ to $112\,\text{ms}$ and filter range from $25\,\text{kHz}$ to $100\,\text{kHz}$

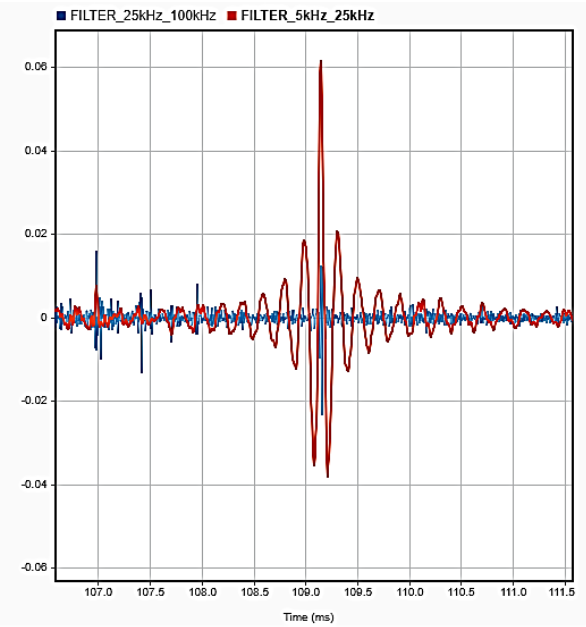



**Fig. C4** AE signal, $tf_2 = 107$ ms to 112 ms and filter range from 5 kHz to 25 kHz

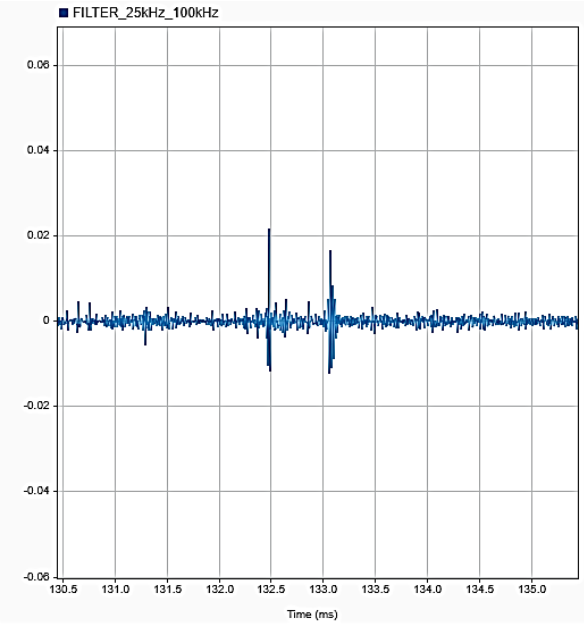



**Fig. C5** AE signal, $tf_3 = 131$ ms to 135 ms and filter range from 25 kHz to 100 kHz

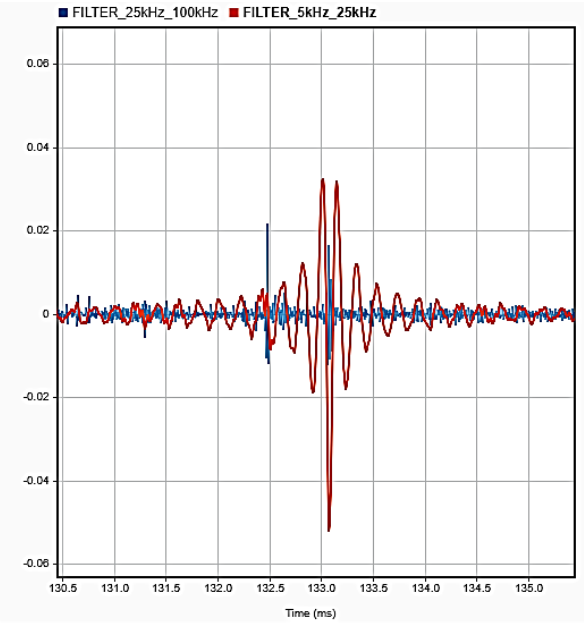



**Fig. C6** AE signal, $tf_3 = 131\,\text{ms}$ to $135\,\text{ms}$ and filter range from $5\,\text{kHz}$ to $25\,\text{kHz}$

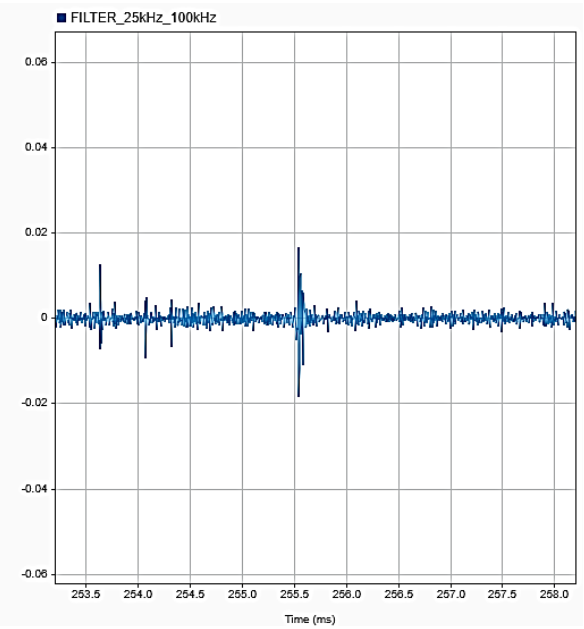



**Fig. C7** AE signal, $tf_4 = 253\,\text{ms}$ to $258\,\text{ms}$ and filter range from $25\,\text{kHz}$ to $100\,\text{kHz}$

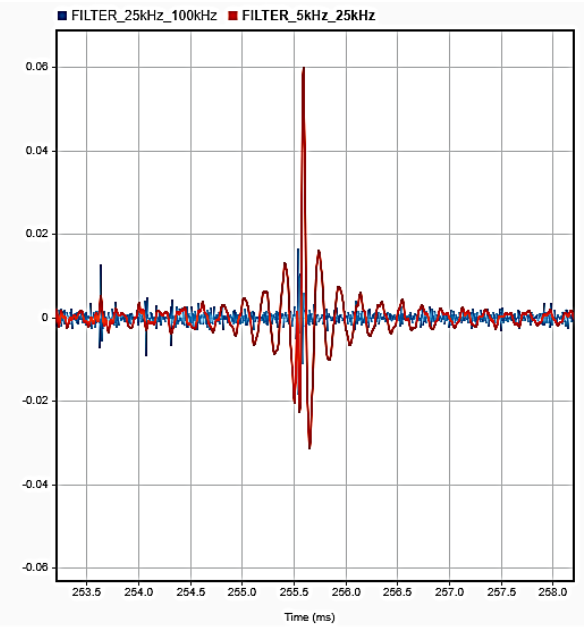



**Fig. C8** AE signal, $tf_4 = 253\,\text{ms}$ to $258\,\text{ms}$ and filter range from $5\,\text{kHz}$ to $25\,\text{kHz}$

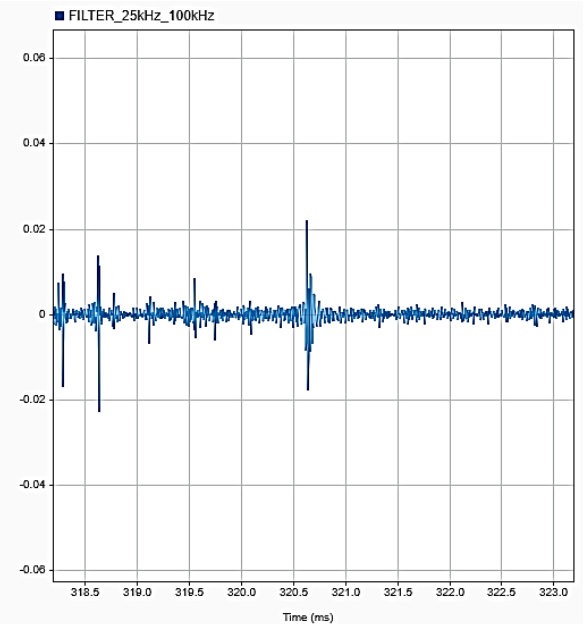



**Fig. C9** AE signal, $tf_5 = 318\,\text{ms}$ to $328\,\text{ms}$ and filter range from $25\,\text{kHz}$ to $100\,\text{kHz}$

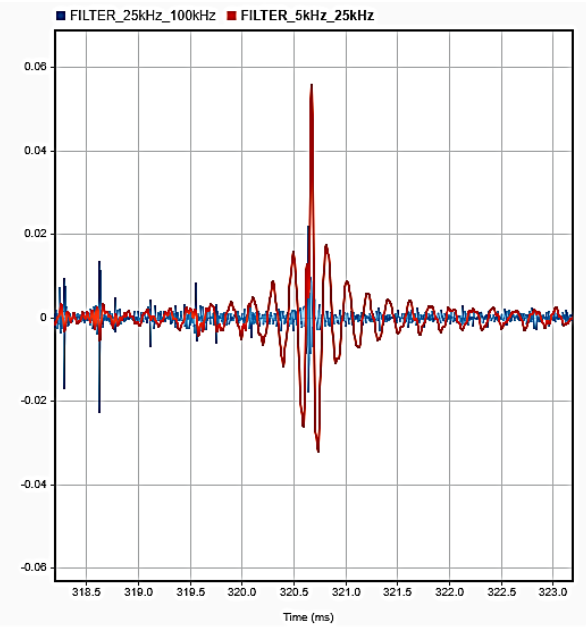



**Fig. C10** AE signal, $tf_5 = 318\,\text{ms}$ to $328\,\text{ms}$ and filter range from $5\,\text{kHz}$ to $25\,\text{kHz}$

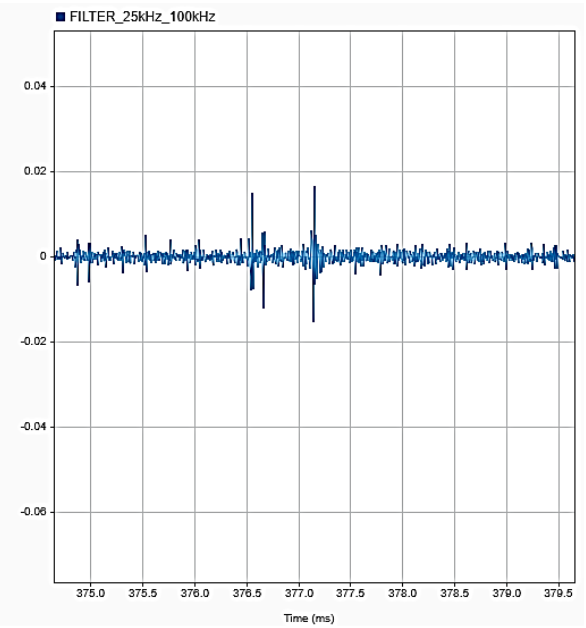



**Fig. C11** AE signal, $tf_6 = 375\,\text{ms}$ to $380\,\text{ms}$ and filter range from $25\,\text{kHz}$ to $100\,\text{kHz}$

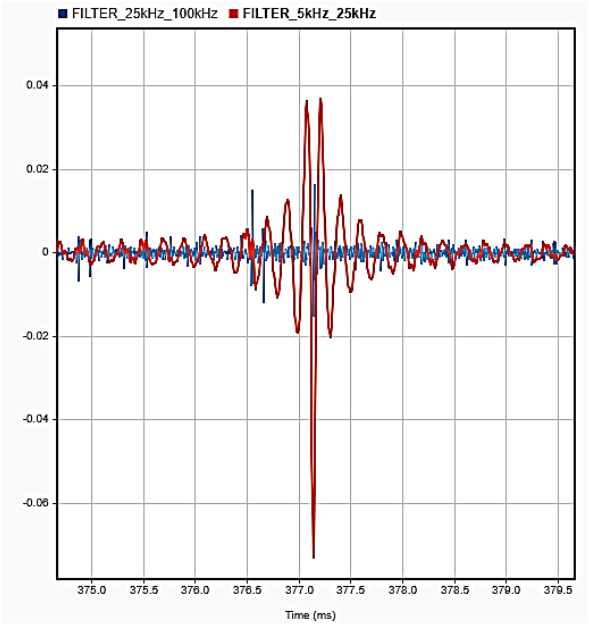



**Fig. C12** AE signal, $tf_6 = 375\,\text{ms}$ to $380\,\text{ms}$ and filter range from $5\,\text{kHz}$ to $25\,\text{kHz}$

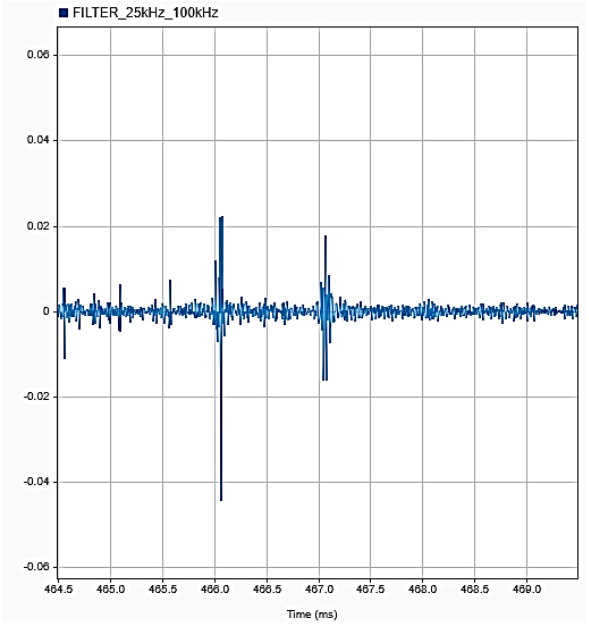



**Fig. C13** AE signal, $tf_7 = 465\,\text{ms}$ to $470\,\text{ms}$ and filter range from $25\,\text{kHz}$ to $100\,\text{kHz}$

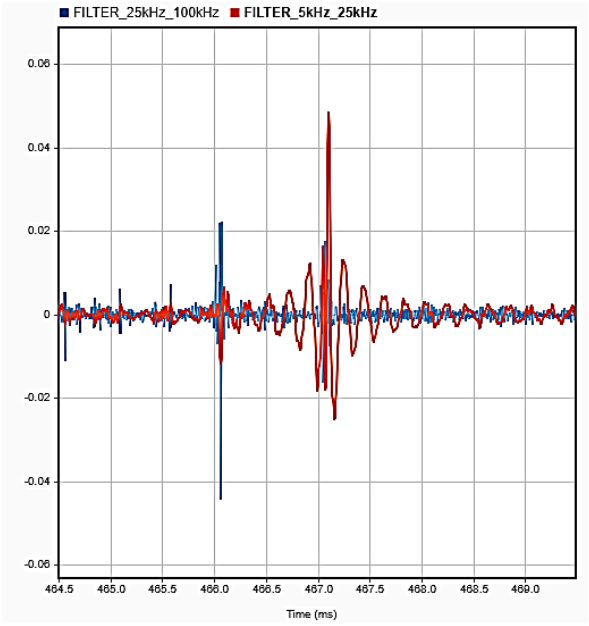



**Fig. C14** AE signal, $tf_7 = 465$ ms to 470 ms and filter range from 5 kHz to 25 kHz

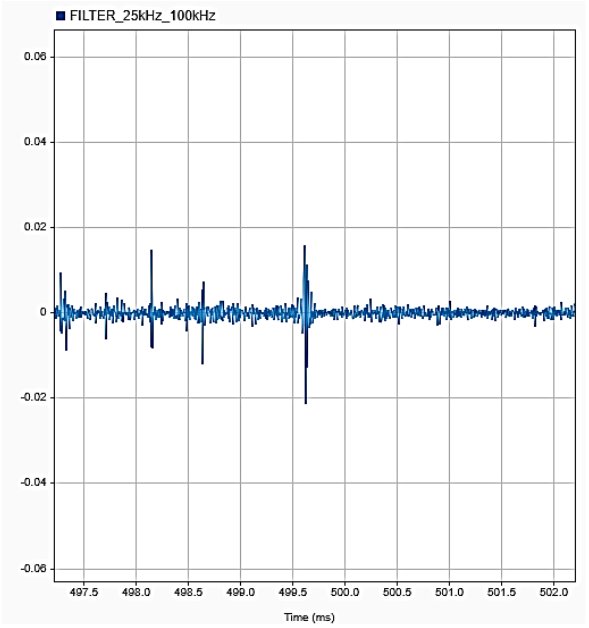



**Fig. C15** AE signal, $tf_8 = 497$ ms to 502 ms and filter range from 25 kHz to 100 kHz

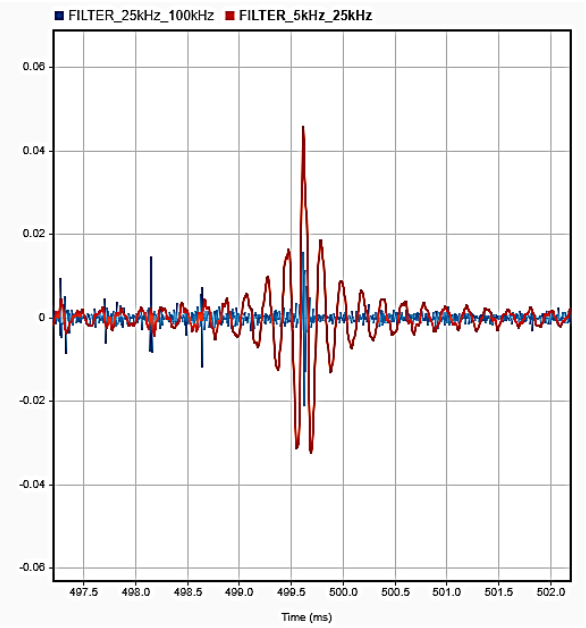



**Fig. C16** AE signal, $tf_8 = 497\,\text{ms}$ to $502\,\text{ms}$ and filter range from $5\,\text{kHz}$ to $25\,\text{kHz}$

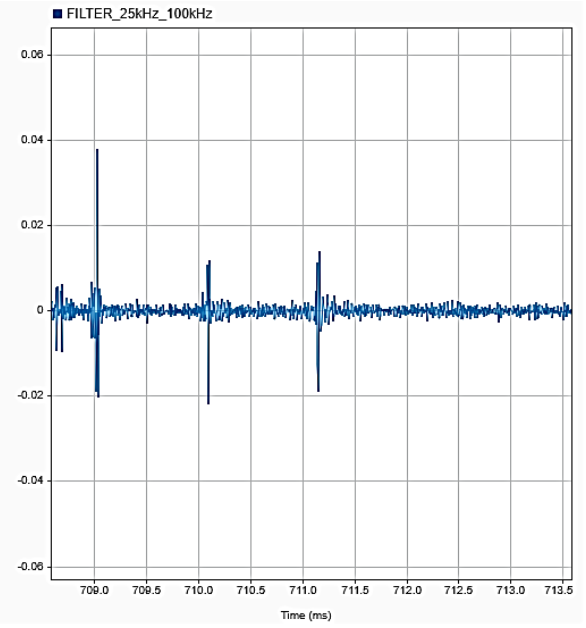



**Fig. C17** AE signal, $tf_9 = 708\,\text{ms}$ to $713\,\text{ms}$ and filter range from $25\,\text{kHz}$ to $100\,\text{kHz}$

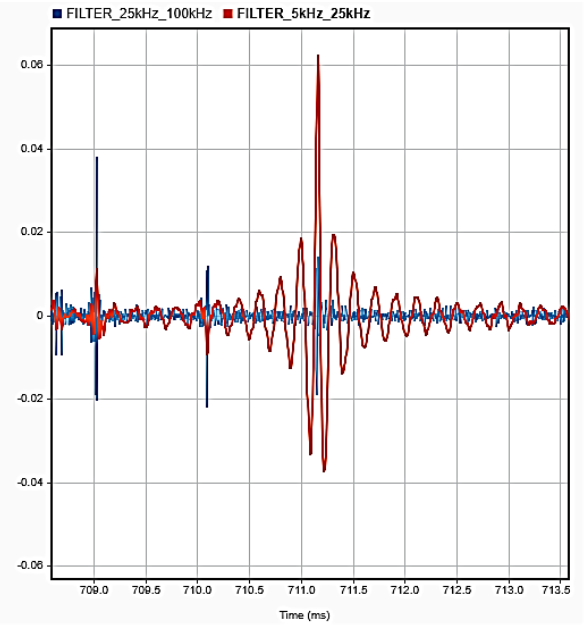



**Fig. C18** AE signal, $tf_9 = 708$ ms to 713 ms and filter range from 5 kHz to 25 kHz

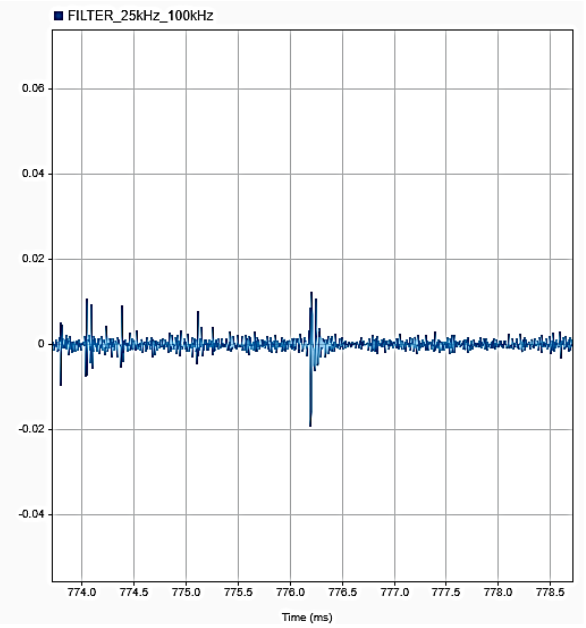



**Fig. C19** AE signal, $tf_{10} = 774$ ms to 779 ms and filter range from 25 kHz to 100 kHz

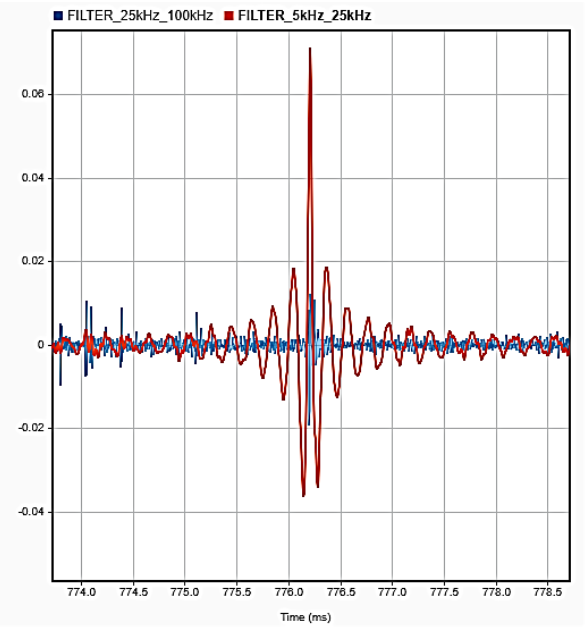



**Fig. C20** AE signal, $tf_{10} = 774$ ms to 779 ms and filter range from 5 kHz to 25 kHz

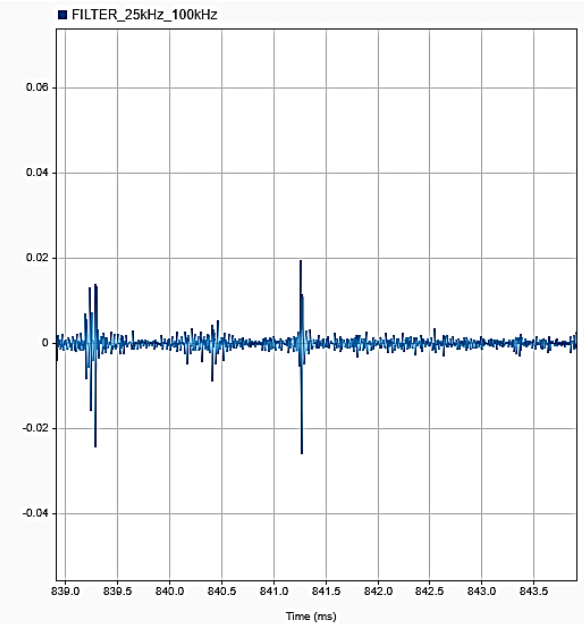



**Fig. C21** AE signal, $tf_{11} = 839$ ms to 844 ms and filter range from 25 kHz to 100 kHz

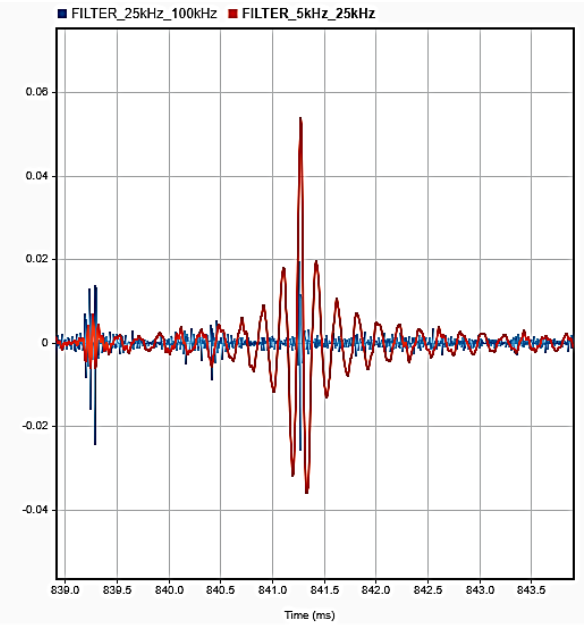



**Fig. C22** AE signal, $tf_{11} = 839$ ms to 844 ms and filter range from 5 kHz to 25 kHz

# References

[1] Katnam, K., Da Silva, L., Young, T.: Bonded repair of composite aircraft structures: A review of scientific challenges and opportunities. Progress in Aerospace Sciences **61**, 26–42 (2013). https://doi.org/10.1016/j.paerosci.2013.03.003

[2] Baker, A.A.: A summary of work on applications of advanced fibre composites at the aeronautical research laboratories, australia. Composites **9**(1), 11–16 (1978). https://doi.org/10.1016/0010-4361(78)90512-8

[3] Baker, A.A.: Bonded composite repair of fatigue-cracked primary aircraft structure. Composite Structures **47**(1), 431–443 (1999). https://doi.org/10.1016/S0263-8223(00)00011-8

[4] Alexander, C., Ochoa, O.O.: Extending onshore pipeline repair to offshore steel risers with carbon–fiber reinforced composites. Composite Structures **92**(2), 499–507 (2010). https://doi.org/10.1016/j.compstruct.2009.08.034

[5] Li, C., Zhao, Q., Yuan, J., Hou, Y., Tie, Y.: Simulation and experiment on the effect of patch shape on adhesive repair of composite structures. Journal of Composite Materials, 1–11 (2019). https://doi.org/10.1177/0021998319853033

[6] Bekas, D.G., Sharif-Khodaei, Z., Aliabadi, F.M.: A smart multi-functional printed sensor for monitoring curing and damage of composite repair patch. Smart Materials and Structures **28**(8), 1–8 (2019). https://doi.org/10.1016/j.compositesb.2019.106945

[7] Bouchiba, M.S.E., Serier, B.: A step towards the optimization of composite bonded repair shape using an estimation distribution approach. Journal of the Brazilian Society of Mechanical Sciences and Engineering **39**, 1755–1771 (2017). https://doi.org/10.1007/s40430-016-0599-2

[8] Katnam, K., Comer, A., Roy, D., Da Silva, L., Young, T.: Composite repair in wind turbine blades: an overview. The journal of Adhesion **91**(1-2), 113–139 (2015). https://doi.org/10.1080/00218464.2014.900449

[9] PETROBRAS: N76: Materiais de Tubulação para Instalações de Refino e Transporte. Petrobras - Petróleo Brasileiro, CONTEC-BR (2016)

[10] API: API-5L: Specification for Line Pipe. American Petroleum Institute API, Washington, D.C. (2004)

[11] PETROBRAS: N2688: Teste de Pressão em Serviço para Vasos de Pressão. Petrobras - Petróleo Brasileiro, CONTEC-BR (2014)

[12] PETROBRAS: N-2555: Inspeção em Serviço de Tubulação (NP-1). Petrobras - Petróleo Brasileiro, CONTEC-BR (20160)

[13] API: API-570 Piping Inspection Code: In-service Inspection, Rating, Repair, and Alteration of Piping Systems. American Petroleum Institute: Washington, D.C., USA (2016)

[14] Sih, G.C.: Mechanics of Fracture Initiation and Propagation: Surface and Volume Energy Density Applied as Failure Criterion vol. 11. Springer, Berlin (2012). https://doi.org/10.1007/978-94-011-3734-8

[15] Zhu, X.-K., Joyce, J.A.: Review of fracture toughness (g, k, j, ctod, ctoa) testing and standardization. Engineering Fracture Mechanics **85**, 1–46 (2012). https://doi.org/10.1016/j.engfracmech.2012.02.001

[16] Mohamadi, A., Behnia, M., Alneasan, M.: Comparison of the classical and fracture mechanics approaches to determine in situ stress/hydrofracturing method. Bulletin of Engineering Geology and the Environment **80**, 3833–3851 (2021). https://doi.org/10.1007/s10064-021-02184-8

[17] ISO: 24817: Petroleum, petrochemical and natural gas industries — Composite repairs for pipework — Qualification and design, installation, testing and inspection. International Organization for Standardization: Vernier, Geneva Switzerland (2017)

[18] ASME: PCC-2: Repair of Pressure Equipment and Piping. The American Society of Mechanical Engineers: New York, NY, USA (2022)

[19] Baker, A.A.: Repair of cracked or defective metallic aircraft components with advanced fibre composites — an overview of australian work. Composite Structures **2**(2), 153–181 (1984). https://doi.org/10.1016/0263-8223(84)90025-4

[20] Baker, A.A., Callinan, R.J., Davis, M.J., Jones, R., Williams, J.G.: Repair of mirage iii aircraft using the bfrp crack-patching technique. Theoretical and Applied Fracture Mechanics **2**(1), 1–15 (1984). https://doi.org/10.1016/0167-8442(84)90035-1

[21] Echer, L.: Uma metodologia para otimização da forma geométrica de reparos em placas laminadas. Doctorate dissertation, Federal University of Rio Grande do Sul (UFRGS), Porto Alegre (Feb 2021)

[22] PLASTEEL: Epoxy resin compound with micro-particulate reinforcement. Datasheet of PLASTEEL-M4:1, Quimatic Tapmtic®, RJ (2021)

[23] Echer, L., Souza, C.E.d., Marczak, R.J.: A study on the best conventional shapes for composite repair patches. Materials Research **24(2)** (2021). https://doi.org/10.1590/1980-5373-MR-2021-0304

[24] ASME: B31.3: Piping Process. The American Society of Mechanical Engineers: New York, NY, USA (2010)

[25] ASME: Section VIII, Division 1: Boiler and Pressure Vessel Code - Rules for construction of pressure vessels. The American Society of Mechanical Engineers: New York, NY, USA (2010)

[26] Rojo Tanzi, B.N.: SOFT-AE: Signal Analysis Software for Acoustic Emission Data, Version 0.4, Computer Software (2021)